A Femtosecond Waveform Transfer Technique Using Type II Second Harmonic Generation

Haifeng Wang and Andrew M. Weiner, *Fellow, IEEE*

***Abstract*—We present a novel waveform frequency conversion technique by type II second harmonic generation (SHG). We have theoretically studied and experimentally demonstrated femtosecond waveform transfer from 800 to 400 nm wavelength by type II SHG in a lithium triborate (LBO) crystal. The output second harmonic (SH) waveform is a temporally magnified or compressed version of the input fundamental waveform, depending on the experimental configuration. Our experiments demonstrate that this technique can transfer not only the intensity profiles of the fundamental waveform, but also the phase profiles. This technique shows promise for programmable generation of shaped ultrafast optical waveforms down to the UV range, where direct pulse shaping is challenging.**

***Index Terms*—Frequency conversion, pulse shaping, second harmonic generation.**

I. Introduction

FEMTOSECOND pulse shaping [1] using spatial light modulators (SLM) is now a widely used technique in ultrafast optics. SLMs are well developed for light in the visible and near-IR range, but are not readily available for shorter and longer wavelengths. Although there has been progress in developing new SLM devices (e.g., MEMS arrays that have been used down to 400 nm [2]), there is interest in developing approaches that convert shaped waveforms to new wavelength ranges. Such waveform transfer was first demonstrated in experiments where shaped near-IR pulses were used to excite photoconductive antennas for shaping and enhancement of ultrafast tetrahertz transients [3]. Several groups have also demonstrated waveform transfer to longer wavelengths via difference frequency generation (DFG) [4]–[7]. To generate shaped waveform at shorter wavelengths, the use of phase-shaped input waveforms during second harmonic generation (SHG) was reported [8], but the scheme did not allow general control of the output waveform. Phase-shaped waveforms from a femtosecond fiber laser have also been used for coherent control of the nonlinear polarization spectrum in SHG, resulting in a novel spectral phase correlator with applications to waveform recognition for ultrafast optical communications [9]. The availability of shaped pulses in the blue, or potentially shorter wavelengths, may open new prospects for coherent and laser machining studies, which are at present usually confined to the 800-nm range of short pulse Ti:sapphire sources.

Manuscript received December 22, 2003; revised March 19, 2004. This work was supported in part by the National Science Foundation under Grant 0100949-ECS and Grant 0203240-ECS.

The authors are with the School of Electrical and Computer Engineering, Purdue University, West Lafayette, IN 47907 USA (e-mail: wangh@ecn.purdue.edu).

Digital Object Identifier 10.1109/JQE.2004.830192

In this paper we demonstrate a novel type II SHG waveform transfer scheme allowing general intensity and phase control of an output second harmonic (SH) waveform. In addition to the main goal of the waveform transfer from the fundamental wavelength to SH wavelength, there are also other interesting phenomena in the process. One phenomenon is the temporal magnification or compression effects resulting from the group velocity mismatch (GVM) between the interacting waves. In this context, the time lens technique [10], [11] which can magnify a waveform through upconversion has been previously been reported. The difference is that the time lens technique uses chirped pulses in upconversion which results in chirped output waveforms and relatively low efficiency, but it can provide large and tunable temporal magnification (more than 100 times magnification [10], [11]). In our technique, both the amplitude and phase profile of the output can be generally controlled without chirp, but the temporal scaling effect from GVM is normally much less significant than in the time lens technique and is not easily tunable. Hence, although this temporal scaling effect arises intrinsically in our waveform transfer scheme, large scaling factor is not a goal our technique is meant to pursue.

Another interesting and potentially useful phenomenon is a temporal filter effect that arises in our technique. The temporal filter window is set by the total GVM between the two input waves in the nonlinear crystal. This effect can be used to remove side lobes or select one part of a long waveform for transfer. This can be useful for applications such as coherent control [12]–[18], in which optical pulse shaping has become a very useful tool, and potentially in laser machining [19]–[22] as well. A key point is that high intensity laser matter interactions are very sensitive to small prepulses; our temporal window effect can remove such prepulses during the waveform transfer process. In some cases, particularly for laser machining which is intensity driven, phase-only pulse shapers should be used instead of phase and amplitude pulse shapers to avoid significant loss. However, the output of a phase-only pulse shaper often contains side lobes before or after the main waveform which may disturb the results. Our technique can be used to upconvert the waveform and remove side lobes at the same time. Also, for laser machining, shorter wavelength light can often be better absorbed by the material and achieve smaller feature sizes; for coherent control, shorter wavelength light can enable higher energy transitions. Because amplified systems are generally used in those applications, our technique should have good conversion efficiency as well (even though the present experiments are performed with a low power femtosecond oscillator). The scaling laws for efficiency and projected examples for amplified pulses are discussed toward the end of this paper.

II. Theory

We use an oeo type II SHG scheme for waveform transfer. There are three interacting waves in the process: the input fundamental ordinary wave (o-wave), the input fundamental extraordinary wave (e-wave) and the output SH o-wave. In a birefringent crystal, o-waves and e-waves have linear polarizations perpendicular to each other. The refractive index of e-wave changes with propagation direction, but that of o-wave does not. First let us define the following notations for the three interacting waves:

$$\widetilde{E}_m(u,\omega) = \widetilde{A}_m(u,\omega)e^{-jk_m(\omega)u} \tag{1}$$

$$A_m(u,t) = \int \widetilde{A}_m(u,\omega)e^{j\omega t}d\omega = a_m(u,t)\exp(j\omega_m t) \tag{2}$$

$$\widetilde{A}_m(u,\omega) = \frac{1}{2\pi}\int A_m(u,t)e^{-j\omega t}dt \tag{3}$$

where u is the direction of propagation, m is a general subscript which can be replaced by o, e, or 2, and subscripts o, e, and 2 represent the fundamental o-wave, the fundamental e-wave, and the SH wave, respectively. ω_m is ω_1 for the fundamental waves, and $2\omega_1$ for the SH wave. So $A_m(u,t)$ is the temporal complex electric field taking out the propagation effects in the material, and $a_m(u,t)$ is the complex amplitude envelope. Assuming plane waves and no source depletion, $A_o(t)$ and $A_e(t)$ are independent of u, and they are the temporal input fields. We can derive the following equation in the frequency domain from basic wave equations [23]:

$$\frac{\partial}{\partial u}\widetilde{A}_2(u,\omega) = -j\left(\frac{\omega}{c}\right)^2 d_{\text{eff}}\frac{e^{jk_2(\omega)u}}{k_2(\omega)} \cdot \left[\int_{-\infty}^{\infty}\widetilde{A}_o(\omega-\omega')e^{-jk_o(\omega-\omega')u}\widetilde{A}_e(\omega')e^{-jk_e(\omega')u}d\omega'\right]. \tag{4}$$

Specifically, we are using the case that one fundamental input is a shaped pulse, and the other is an unshaped short pulse (called the reference pulse). If the reference pulse is much shorter than the waveform of the shaped pulse, it can be treated as a δ pulse in the integral of (4). There are two possibilities: the fundamental o-wave is the reference pulse or the fundamental e-wave is the reference pulse. Here we study the first case first. If we let the fundamental o-wave be a δ function (let $\widetilde{A}_o(\omega) \equiv \sigma$ in (4), where σ is the pulse area and has the unit of field $\times$ time), the integral in (4) would be

$$\sigma\int_{-\infty}^{\infty}\widetilde{A}_e(\omega')\exp[-ju(k_o(\omega-\omega')+k_e(\omega'))]d\omega'. \tag{5}$$

We can expand the wave vectors as functions of frequency ignoring GVD

$$k_o(\omega-\omega') = k_o + \frac{1}{V_o}(\omega-\omega'-\omega_1) \tag{6}$$

$$k_e(\omega') = k_e + \frac{1}{V_e}(\omega'-\omega_1) \tag{7}$$

$$k_2(\omega) = k_2 + \frac{1}{V_2}(\omega-2\omega_1). \tag{8}$$

where k_o, k_e, and k_2 are the wave vectors of the three waves at center frequencies, respectively. V denotes the group velocity, and we define the GVM between any two waves as

$$\beta_{pq} = \frac{1}{V_p} - \frac{1}{V_q} \tag{9}$$

where p and q can be o, e, or 2. The integral of (5) can be written as

$$\sigma\cdot\exp\left[-ju\left(k_o+k_e+\frac{1}{V_o}(\omega-2\omega_1)+\beta_{oe}\omega_1\right)\right] \cdot\int_{-\infty}^{\infty}\widetilde{A}_e(\omega')\exp(ju\beta_{oe}\omega')d\omega' = \sigma\cdot A_e(\beta_{oe}u)\exp\left[-ju\left(k_o+k_e+\frac{1}{V_o}(\omega-2\omega_1)+\beta_{oe}\omega_1\right)\right]. \tag{10}$$

We have used the Fourier transform (2). By bring the above result into the partial differential (4) and using the phase matching condition at center frequencies $k_2 = k_o + k_e$, we obtain

$$\frac{\partial}{\partial u}\widetilde{A}_2(u,\omega) = l-j\left(\frac{\omega}{c}\right)^2\frac{d_{\text{eff}}\sigma}{k_2(\omega)}A_e(\beta_{oe}u) \times\exp[ju(\beta_{2o}(\omega-2\omega_1)-\beta_{oe}\omega_1)]. \tag{11}$$

Assuming that the crystal is from $u=0$ to $u=z$, the output SH spectrum is the integral of the above equation

$$\widetilde{A}_2(z,\omega) = -j\left(\frac{\omega}{c}\right)^2\frac{d_{\text{eff}}\sigma}{k_2(\omega)} \cdot\int_0^z A_e(\beta_{oe}u)\exp[ju(\beta_{2o}(\omega-2\omega_1)-\beta_{oe}\omega_1)]du. \tag{12}$$

If the crystal is much longer than the interaction length of type II SHG, the integral would be the same as if the boundaries are infinity, then we can use the Fourier transform (3) to get the output SH spectrum

$$\widetilde{A}_2(\omega) = -j\left(\frac{\omega}{c}\right)^2\frac{d_{\text{eff}}\sigma}{k_2(\omega)}\frac{2\pi}{|\beta_{oe}|}\widetilde{A}_e\left(\frac{\beta_{2o}}{\beta_{eo}}(\omega-2\omega_1)+\omega_1\right). \tag{13}$$

Note that $\widetilde{A}_e(\omega)$ is centered at ω_1, and $\widetilde{A}_2(\omega)$ is obviously centered at $2\omega_1$. Using Fourier transform again, we can find the temporal SH field

$$A_2(t) = jd_{\text{eff}}\frac{2\pi\sigma}{|\beta_{oe}|\,c}\int\frac{\omega}{n_2(\omega)}\widetilde{A}_e\left(\frac{\beta_{2o}}{\beta_{eo}}(\omega-2\omega_1)+\omega_1\right)e^{j\omega t}d\omega. \tag{14}$$

Assuming that $\omega/n_2(\omega) \approx \omega_2/n_2$ is almost constant within the SH spectrum and can be brought out of the integral, and using (2) to replace $A(t)$ with $a(t)$, we have

$$a_2(t) = -jd_{\text{eff}}\frac{2\pi\sigma}{|\beta_{oe}|\,c}\frac{\omega_2}{n_2}a_e\left(\frac{\beta_{eo}}{\beta_{2o}}t\right). \tag{15}$$

From (15), the output SH amplitude waveform is a directly scaled version of the shaped fundamental waveform when the

input o-wave is a δ function. In the other case, if the fundamental e-wave is the reference pulse instead and the fundamental o-wave is the shaped waveform, we will similarly get

$$a_2(t) = -jd_{\text{eff}}\frac{2\pi\sigma}{|\beta_{eo}|\,c}\frac{\omega_2}{n_2}a_o\left(\frac{\beta_{oe}}{\beta_{2e}}t\right). \tag{16}$$

Again the output SH waveform is a scaled version of the shaped input waveform but with a different scaling factor. In our experiments, we use type II SHG in an lithium triborate (LBO) crystal at 805 nm. The crystal orientation is $\theta = 76.88^\circ$ and $\phi = 90^\circ$ (YZ plane). Based on the dispersion equations of LBO [24], the inverse group velocities of the three interacting waves are: $V_o^{-1} = 5289$ fs/nm, $V_e^{-1} = 5435$ fs/nm, $V_2^{-1} = 5472$ fs/nm. So in (15), we have $\beta_{eo} = 146$ fs/nm, $\beta_{2o} = 183$ fs/nm, and $\beta_{eo}/\beta_{2o} = 0.8$. The SH waveform is a temporally magnified version of the shaped input waveform, and the magnification factor is 1.25. In (16) $\beta_{oe} = -146$ fs/nm, $\beta_{2e} = 37$ fs/nm and $\beta_{oe}/\beta_{2e} = -4$. The SH waveform is a compressed and time reversed version of the shaped input waveform, and the compression factor is 0.25. According to (15) and (16), when the reference pulse is a δ function, the shaped input field profile will be transferred to the SH field including both amplitude and phase. When the reference pulse is not a δ function, there will be a convolution effect, but the scaling factors for waveform transfer are still true for features longer than the reference pulse.

We can also inspect these temporal scaling effects from another point of view. If both fundamental inputs are identical single pulses, then the time when the SH pulse leaves the crystal is related to the times when the two input pulses enter the crystal by a linear equation, and the corresponding linear factors should equal the above magnification and compression factors. The mathematical derivation is as follows. Assuming that the fundamental o-pulse enters the crystal at t_o and the fundamental e-pulse enters at t_e, they will meet in the crystal at length l_1 and time t_1, which can be calculated from their group velocities

$$l_1 = (t_o - t_e)\left(\frac{1}{V_e} - \frac{1}{V_o}\right)^{-1} = \frac{t_o - t_e}{\beta_{eo}} \tag{17}$$

$$t_1 = t_e + \frac{l_1}{V_e} = t_o + \frac{l_1}{V_o} = \frac{t_o}{V_e\beta_{eo}} - \frac{t_e}{V_o\beta_{eo}}. \tag{18}$$

The SH pulse is then generated at time t_1 and location l_1, and travels at its own group velocity V_2 to the output end. The time when the SH pulse leaves the crystal is

$$t_2 = t_1 + \frac{L - l_1}{V_2} = \frac{\beta_{2o}}{\beta_{eo}}t_e + \frac{\beta_{e2}}{\beta_{eo}}t_o + \frac{L}{V_2}. \tag{19}$$

L is the crystal length. The two linear factors here β_{2o}/β_{eo} and β_{e2}/β_{eo} are the same as what we can derive from (15) and (16). Note that the sum of the two factors is always 1 since $\beta_{2o}/\beta_{eo} + \beta_{e2}/\beta_{eo} = \beta_{eo}/\beta_{eo} = 1$. If the fundamental o-pulse is faster than the e-pulse in the crystal, we must have $t_o > t_e$ or they will not interact. For the type II SHG in LBO we are studying, ignoring the constant time delay L/V_2, we have

$$t_2 = 1.25t_e - 0.25t_o. \tag{20}$$

From this relationship, if we temporally delay the input e-pulse, the SH pulse will also be delayed, and the amount of its delay is 1.25 times of the e-pulse delay; if we temporally delay the input o-pulse, the SH pulse will actually be advanced in time, which is a negative delay 0.25 times of the o-pulse delay. This is a seemingly strange phenomenon. It can be explained by the fact that the fundamental o-pulse has the fastest speed in the crystal. Although delaying it causes the SH pulse to be generated later in crystal, it is also generated closer to the output end of the crystal, so in the end the SH pulse leaves the crystal earlier! Equation (20) is easy to verify experimentally, as we will see in the next section.

These temporal scaling effects are used in our scheme to transfer a shaped pulse waveform. The physical picture: due to the temporal walkoff between the shaped input waveform and the reference pulse caused by GVM, SHG between the reference pulse and different parts of the shaped waveform happens at different longitudinal locations of the crystal. The nonlinear polarization in space is then a scaled version of the temporal profile of the shaped input (assuming a δ function reference), and the output SH field in time is a scaled version of the nonlinear polarization in space. A related picture applies to the shaped pulse DFG experiments of [4], where shaped pulses in the mid-IR were generated. There is also some analogy to experiments on pulse shaping in type I SHG using modulated gratings in PPLN [25], where different slices of the SH temporal waveform also arise at different longitudinal locations of the grating, with a scaling factor dependent on the GVM between the fundamental and SH fields. Our work is similar in this sense. However, in [25] the output waveform is basically determined by the PPLN structure. If a different output waveform is desired, one would need to use a different waveguide. In our scheme, we have programmable optical control through the interaction between the reference pulse and a shaped waveform.

Since the temporal walkoff in a crystal is finite, if the reference pulse enters the crystal at a fixed time, the shaped waveform must enter the crystal within a certain time window to interact with it. We call this time window the *interaction window*, whose length is the total temporal walkoff in crystal between the inputs. For our 10–mm LBO crystal, the length of the interaction window is 146 fs/nm $\times$ 10 mm $= 1.46$ ps.

There are two other factors which may limit the interaction length. The first is the spatial walkoff between the fundamental e-wave and o-waves—their energy flows in slightly different directions, the angle between which is the walkoff angle. The spatial walkoff can also separate the two inputs and reduce the interaction window. It sets a lower limit of the input beam size. The walkoff angle in our LBO is 0.24°, and the total spatial walkoff is $L\tan\rho = 42$ μm. So our beam should be larger than that size, which is true in our experiments. The second factor is the beam diffraction. For focused beams, the diffraction can cause the beam size to increase significantly when propagating in the crystal and the SHG efficiency will roll off due to lower field intensity. The output SH waveform is then modulated by the nonuniform efficiency profile in the interaction window. This phenomenon exists in our experiments, as we will describe in the next section.

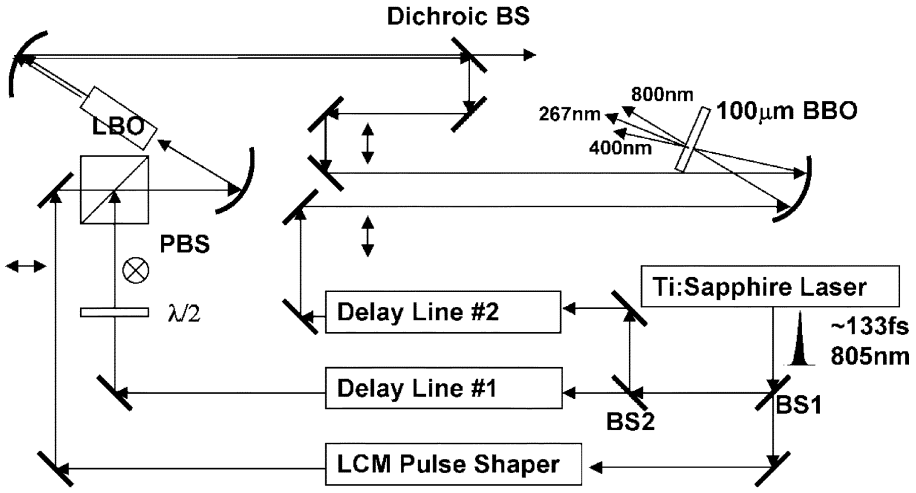

Fig. 1. Experimental setup of type II SHG experiments. BS: beam splitter; LCM: liquid crystal modulator; $\lambda/2$: half wave plate; PBS: polarization beam splitter.

There are several possibilities to remove the nonuniform efficiency profile. First, as we mentioned in the introduction section, some applications often use amplified systems. In that case, unfocused beams could be used for type II SHG with good efficiency; both the diffraction and spatial walkoff would be negligible, and the efficiency would likely be uniform. Second, it maybe possible to use waveguide geometry for waveform transfer. Neither spatial walkoff nor beam diffraction should be a problem in waveguides, therefore, the efficiency would be expected to be uniform. Also, the nonuniform efficiency profile can be taken into account when programming the shaped input waveform if a certain output waveform is desired.

III. Experiments

Our setup is shown in Fig. 1. The source is a mode-locked Ti:sapphire laser, horizontally polarized, with 133-fs FWHM intensity duration, 805-nm center wavelength and 88-MHz repetition rate. It is split into three arms by two beam splitters (BS). One arm goes through a traditional Fourier-transform pulse shaper, which uses a 512-element phase-only liquid crystal modulator (LCM) [26] provided by Raytheon Company. This is the shaped waveform input of type II SHG. The arm with delay line #1 is the reference pulse input of type II SHG. The arm with delay line #2 is for cross-correlation measurement with the output blue waveform. The reference pulse has its polarization rotated 90° by a half-wave plate, and recombined collinearly with the waveform input by a polarization beam splitter (PBS). Thus, the polarizations of the two inputs are perpendicular. In crystal one of them is an o-wave and the other is an e-wave. We can switch o-wave and e-wave by using another half-wave plate after the PBS. They are focused into the 10 mm LBO by a spherical mirror with 225-mm focal length. The LBO crystal was cut for type II SHG at 800 nm with orientation $\theta = 76.88°$ and $\phi = 90°$ (YZ plane), as we mentioned before. Another spherical mirror with 37.5 mm focal length collects the output. The blue output is separated from the red light by two dichroic beam splitters, and then directed to a 100 μm beta-barium borate (BBO) crystal for intensity cross-correlation measurements, using the unshaped red pulse from delay line #2 as a reference for sum-frequency generation (SFG). The GVM between the 800 nm input and the 400 nm input in the BBO crystal is 327 fs/mm; this results in ~33 fs group velocity walkoff, which is sufficiently small that it does not affect the accuracy of our intensity cross-correlation measurements. The generated UV signal at ~267 nm is measured by a photo-multiplier tube (PMT).

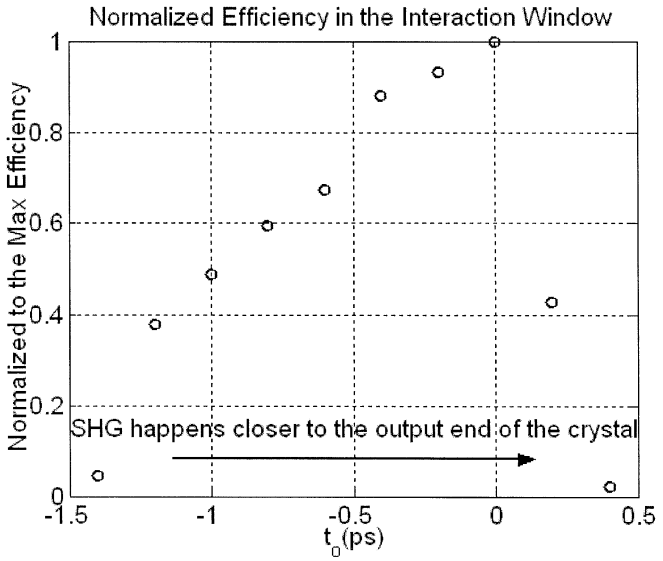

Fig. 2. Change of type II SHG efficiency in the interaction window. The x-axis is t_o relative to the maximum efficiency point while t_e is fixed. The y axis is the efficiency normalized to the maximum efficiency.

We measured the nonuniform efficiency profile in the interaction window and the results are shown in Fig. 2. Both fundamental inputs are unshaped single pulses in this experiment. In Fig. 2, the y axis is the measured efficiency normalized to the maximum efficiency. The maximum efficiency is 1.3×10^{-4} when o-wave and e-wave pulses each have 38 mW average power. The x axis is the relative time when the o-pulse enters the crystal, and the later the time is, the closer to the output end of the crystal SHG occurs. Here, based on our measurements, SHG has the maximum efficiency when it happens near the output end of the crystal, and it drops to about 40% of

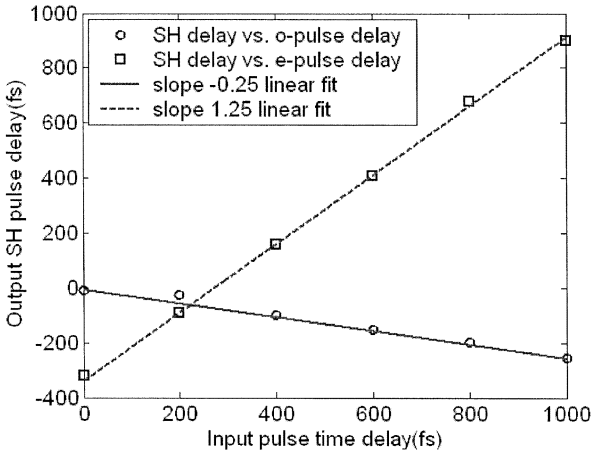

Fig. 3. Dependence of the SH pulse delay on the two input pulse delays.

the maximum efficiency when it happens near the input end of the crystal. Assuming Gaussian beam inputs, the confocal parameter ($b = 2\pi n w_0^2/\lambda$) in the crystal is estimated to be about 8.9 mm. So the beam area can double in the 10-mm crystal length, reducing the efficiency by 50%, which can roughly explain the efficiency roll-off.

First we will show results verifying (20), the relationship between the input and output pulse delays. In these experiments, we observe the peak delay of the output SH pulse while changing the delay of one of the input pulses. The results are shown in Fig. 3. As we can see, the measured relationships between the SH pulse delay and the input pulse delays agree with the linear fits extremely well. This undoubtedly proves (20) and our analysis of the temporal scaling effects.

Fig. 4 shows some demonstrations of waveform transfer. In Fig. 4(a), the shaped red waveform (top figure) mainly consists of two asymmetrical pulses, the interval between which is 980 fs. In the magnification configuration (middle figure), the blue waveform shows two asymmetrical pulses in the same order. The interval is 1.22 ps, and the factor $1.22/0.98 = 1.245$ matches the predicted 1.25 very well. In the compression configuration (bottom figure), a half-wave plate is used after the PBS in our setup (Fig. 1) to switch the input e-wave and o-wave. Two asymmetrical pulses are in reversed order as predicted. The interval between them is so small that they have partially merged. The interval between the peaks is 260 fs and the factor $26/98 = 0.265$ also matches the predicted 0.25 very well.

One might notice that although the interval between the pulses is stretched or compressed as predicted, the individual pulse shape is not transferred following the predicted scaling factors. This is because the reference pulse is not a δ function. Here, it has the same duration as an individual pulse in the shaped waveform, and the duration of the output SH pulse involves a convolution effect which cannot be predicted by the scaling factors from group velocities.

We can also see the modulation effect of the nonuniform efficiency profile in the interaction window from Fig. 4(a). In the magnification configuration, the shaped red waveform is e-wave, which is slower than the reference pulse. And so the transfer of the earlier (higher) pulse happens closer to the output end of the crystal, which got higher efficiency than the later (lower) pulse. As a result in the middle figure, the difference of peak heights is increased. In the compression configuration, the roles of the red o-wave and e-wave are switched and the opposite happens. So, in the bottom figure, the difference of peak heights is decreased.

In Fig. 4(b), the shaped red waveform (top figure) mainly consists of three pulses with decreasing heights. The interval between the leftmost and rightmost peak is 980 fs. The output with the magnification configuration is in the bottom figure. The three pulses are transferred, and the interval is stretched to 1.212 ps. The factor $1.212/0.98 = 1.24$ also matches 1.25 very well. The nonuniform efficiency profile also increases the differences between peak heights in this case. We did not demonstrate waveform-compression using the 3-peak waveform in Fig. 4(b) because all three pulses would merge into one broad peak. Note that the small ripples at -1 and $+2$ ps in the shaped red waveform no longer show up in the output because they are out of the interaction window. This shows that this technique can also serve as a temporal filter.

In the above experiments, the main part of the shaped input is within the interaction window, which is 1.46 ps long. If the shaped input waveform is longer than the interaction window, we can selectively transfer part of the waveform by tuning the delay between the input waveform and the reference pulse, thus, moving the temporal region of the interaction window. A demonstration with the magnification configuration is shown in Fig. 5. The top figure is the shaped red waveform. In the middle figure, the interaction window is approximately -1.2–0.3 ps for the shaped input, and the three pulses at -1.1, -0.6, and 0 ps are transferred. In the bottom figure, the interaction window is approximately 0.3–1.8 ps, and the three pulses at 0.5, 1.1, and 1.7 ps are transferred. This again shows that our scheme has the function of temporal filtering.

We have demonstrated the transfer of intensity profiles. However, based on (15) and (16), presumably our scheme should be able to transfer the phase profile as well. Those two equations showed that if the reference pulse is a temporal delta function, the temporal phase profile of the shaped fundamental pulse will also be copied to the output SH waveform, satisfying the same magnification or compression factor as the intensity profile. In our experiments, the reference pulse cannot be treated as a delta function, and so the phase profile of the shaped fundamental pulse is averaged over the reference pulse when it is transferred to the SH output.

We have designed an experiment to demonstrate that a linear chirp can be transferred from the shaped fundamental pulse to the SH pulse. The idea is that we can use the LCM pulse shaper to add an up chirp or a down chirp to broaden the fundamental e-pulse while keeping the fundamental o-pulse unaffected. In that sense the o-pulse is the reference here and this is still the magnification configuration. We can control the amount of up chirp and down chirp so that the broadened pulses have approximately the same duration in both cases. After type II SHG with the reference pulse, the output SH pulses should also have similar intensity durations in both cases, because we know that the intensity profiles are transferred, but we need to prove that they carry up chirp or down chirp according to the chirped

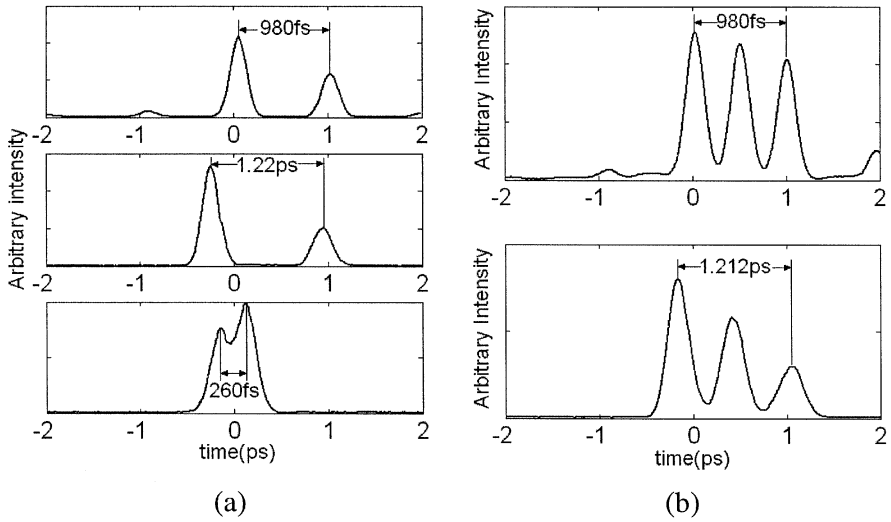

Fig. 4. The waveform transfer from near IR to blue light. (a) top: the fundamental waveform; middle: the SH waveform using magnification configuration; bottom: the SH waveform using compression configuration. (b) top: the fundamental waveform; bottom: the SH waveform using magnification configuration.

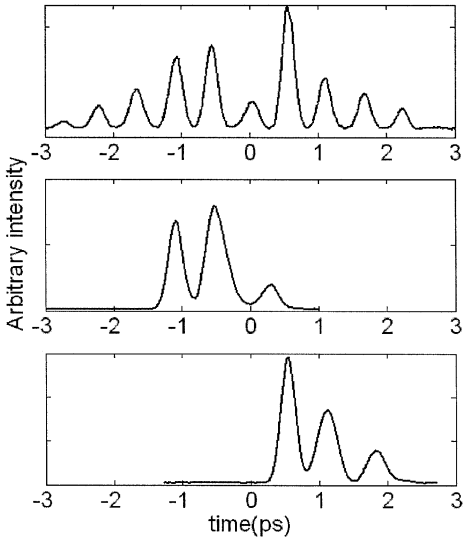

Fig. 5. Demonstration of selectable interaction window in the waveform transfer process using the magnification configuration. Top: fundamental waveform; middle: SH waveform with $-1.2 \sim 0.3$ ps interaction window; bottom: SH waveform with $0.3 \sim 1.8$ ps interaction window.

fundamental pulses. To demonstrate this, we let the SH pulse go through a normal dispersive medium which will add an up chirp to the pulse due to normal dispersion. If the SH pulse is originally down-chirped, the dispersive medium should compress the pulse and make it shorter; if the SH pulse is originally up-chirped, the dispersive medium will further broaden the pulse. If we observe these phenomena, they are a strong evidence that the phase profiles of the fundamental waveform are also transferred to the SH waveform.

In the experiments, we placed two prisms together using index matching gel to serve as the dispersive medium. The material is LaSFN9 glass, and the thickness is 26 mm. The total linear dispersion (or quadratic spectral phase) added by the glass at 400 nm wavelength is calculated to be $\partial^2\phi/\partial\omega^2 = -1.63 \times 10^4$ fs^2 (negative means up chirp). The quadratic spectral phase added by the LCM at 800 nm is calculated to be $\partial^2\phi/\partial\omega^2 = 9.05 \times 10^3$ fs^2 (down chirp). The bandwidth of the source laser is 4.6 THz. The phase transfer here cannot be determined by (15) or (16) because our reference is not narrow comparing with the waveform. We did numerical simulations, which show that the spectral quadratic phase in the SHG output is about 1.6 times of the fundamental chirp. So we have 9.05×10^3 fs^2 $\times$ $1.6 = 1.45 \times 10^4$ fs^2, which roughly meets the calculated glass dispersion. The experimental results are shown in Fig. 6.

In Fig. 6(a), we show the cross-correlation traces of the transform-limited (solid line) and the down-chirped (dashed line) fundamental pulse. The numbers shown in the figures are all the FWHM width of the traces. The fundamental pulse is obviously broadened by the chirp. In Fig. 6(b), three traces of the SH pulse are shown. The solid curve is the trace of the SH pulse generated by the transform-limited fundamental pulse (no prism glass), and the width is 210 fs. The dashed curve is generated by the down-chirped fundamental pulse (no prism glass), and it is broadened to 338 fs. The dotted curve is the trace of the SH pulse generated by the down-chirped fundamental pulse but after it passes the prism glass, and we can see that it is compressed to 214 fs, almost as short as the transform-limited trace. This clearly proves that the SH pulse generated by the down-chirped fundamental pulse is also down chirped.

Fig. 6(c) and (d) shows an experiment in which the fundamental pulse is up chirped, which is in contrast with Fig. 6(a) and (b). In Fig. 6(c), we see that the up-chirped fundamental pulse has approximately the same duration as the down-chirped pulse in Fig. 6(a). In Fig. 6(d), the trace of the SH pulse generated by the up-chirped fundamental pulse (no prism glass) has a width of 353 fs, which is very close to the 338 fs trace in Fig. 6(b). However, after it passes the prism glass, the trace is further broadened instead of compressed. Comparing the two experiments in Fig. 6, we can conclude that the linear chirp in the shaped fundamental pulse was transferred to the SH waveform by type II SHG. This provides clear evidence that the phase profile of the shaped fundamental input can also be transferred by this technique.

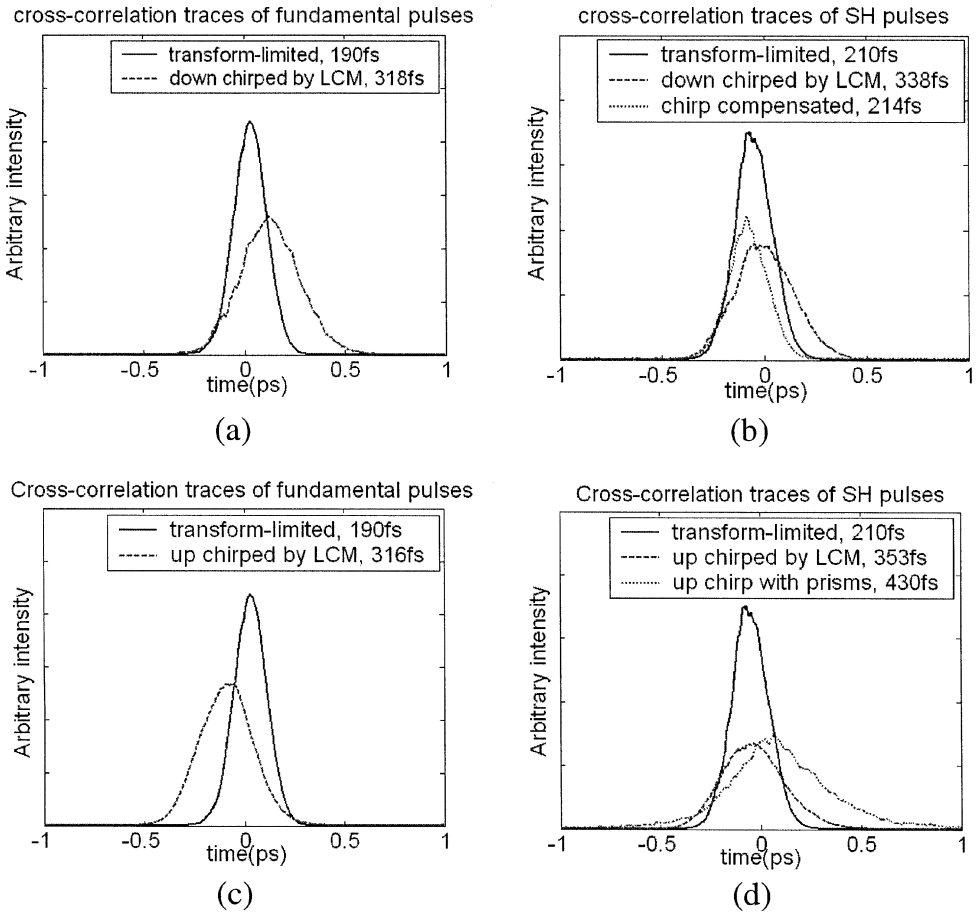

Fig. 6. Demonstration of phase transfer.

IV. Discussion

It is worth discussing the efficiency of the waveform transfer process. In our experiments the fundamental o-pulse and e-pulse have basically the same duration. We can theoretically estimate the conversion efficiency by assuming both input fields are transform-limited Gaussian in time and Gaussian in space

$$A_m(x,y,t) = E_{m-\text{peak}} \exp\left(-\frac{t^2}{t_0^2}\right) \exp\left(-\frac{x^2+y^2}{w_0^2}\right) \exp(j\omega_1 t) \quad (21)$$

where m can be o or e. t_0 is the Gaussian pulse time constant which is related to FWHM intensity duration t_p by $t_p = t_0(2\ln 2)^{1/2}$. w_0 is the e^{-2} intensity beam radius. We ignore beam diffraction and spatial walkoff in the theoretical derivation. The Fourier transform defined by (3) gives

$$\widetilde{A}_m(x,y,\omega) = \frac{E_{m-\text{peak}}}{2\sqrt{\pi}} t_0 \exp\left(-\frac{(\omega-\omega_1)^2 t_0^2}{4}\right) \exp\left(-\frac{x^2+y^2}{w_0^2}\right). \quad (22)$$

We substitute these input field spectra into (4), and after some algebra we find

$$A_2(x,y,t) = -j\kappa \frac{\sqrt{\pi} t_0 E_{o-\text{peak}} E_{e-\text{peak}}}{\sqrt{\beta_{2e}^2+\beta_{2o}^2}} \cdot \exp\left(-\frac{\beta_{oe}^2 t^2}{(\beta_{2e}^2+\beta_{2o}^2)t_0^2}\right) \times \exp\left(-\frac{2(x^2+y^2)}{w_0^2}\right) \exp(2j\omega_1 t) \quad (23)$$

where $\kappa = \omega_2 d_{\text{eff}}/n_2 c$ is the coupling coefficient. We can calculate the input and output pulse energies by integrating field intensity

$$U_m = \frac{1}{2}\varepsilon_0 cn \int_{-\infty}^{\infty} dx \int_{-\infty}^{\infty} dy \int_{-\infty}^{\infty} dt\, |A_m(x,y,t)|^2 \quad (24)$$

where m can be o, e, or 2. We assume $n_o \approx n_e \approx n_2 = n$. The final result is

$$U_2 = \sqrt{\frac{\pi}{\ln 2}} \frac{\gamma t_p}{b|\beta_{oe}|\sqrt{\beta_{2o}^2+\beta_{2e}^2}} U_o U_e \quad (25)$$

where $\gamma = 4\kappa^2/\varepsilon_0 c\lambda_1$. λ_1 is the fundamental wavelength in vacuum. $b = 2\pi n w_0^2/\lambda_1$ is the depth of focus. For our experiments, we use $d_{\text{eff}} = 0.152$ pm/V [27], $b = 8.9$ mm, $t_p = 133$ fs, $U_o = U_e = 0.43$ nJ. The GVM values are given under (16). Equation (25) gives $U_2 = 9\times10^{-4}$ nJ, and the corresponding efficiency U_2/U_o or U_2/U_e is 0.002. This is roughly one order of magnitude higher than the experimental value of 1.3×10^{-4}. Possible reasons of this difference are lack of perfect spatial overlap, spatial walkoff, beam diffraction and the aberration caused by the spherical mirrors used to focus the beams into the crystal. None of these factors were accounted for in the theoretical calculation.

Our technique should be easily extendable to amplified laser systems which will provide much higher conversion efficiency. For example, if we were using an amplified system providing the same average power (38 mW average power for each input) and

1 kHz repetition rate, the pulse energy would be 10^5 higher. In that case we can simply use flat mirrors to direct the beam into the type II SHG crystal instead of the spherical mirrors in the setup Fig. 1. Assuming that we control the beam size so that the e^{-2} intensity beam radius is 1 mm, from our experimental efficiency 1.3×10^{-4} and focused beam radius 27 μm, we can estimate the efficiency with amplified pulses to be roughly 1%. With the 1–mm beam radius, the confocal parameter of the Gaussian beam would be about 12 meters, while the crystal is only 10-mm long and the total spatial walkoff is only 42 μm as we mentioned. So the beam diffraction and spatial walkoff could be totally ignored, and we can expect a uniform efficiency of 1% in the interaction window as long as the two inputs are aligned well. It should be reasonable to get several tens of percent efficiency by slight focusing and using higher pulse energies, since amplified systems can now relatively routinely provide up to $\sim$1-mJ pulse energy which is much higher than we assumed (38 μJ).

We note that our technique is related to previous work of waveform transfer into the mid-IR using DFG [4], in the sense that the GVM between interacting waves is utilized there also. It is also directly extendable to other three-wave mixing processes such as SFG. As long as there is GVM between the two inputs, they do not need to have different polarizations. And the output could have even shorter wavelengths. For example, it is possible that one can use an 800-nm +400 nm => 267 nm ooe SFG in BBO crystal to transfer a waveform from 800 to 267 nm (UV). In that case the phase matching angle is 43.3°; the 800-nm pulse is the fastest and the 267-nm pulse is the slowest; the GVM between the 800-nm and 400-nm inputs is 327 fs/mm; the GVM between the 400-nm input and 267-nm output is 420 fs/mm. So when the waveform is transferred from 800 to 267 nm in this process, the 267-nm waveform is a magnified and time-reversed version of the 800-nm waveform, and the temporal scaling factor is $-420/327 = -1.28$.

V. Conclusion

In summary, we have demonstrated femtosecond waveform transfer from the near IR to the blue by type II SHG. We have shown that the output SH waveform can be a magnified or compressed version of a shaped input waveform depending on the configuration. The theory predicts and the experiments confirm that both the intensity and the phase profile of the shaped input waveform can be transferred. The interaction window can be increased by using longer crystals or crystals with larger GVMs. The temporal filter effect of our technique can be used to remove the side lobes of a waveform in the upconversion process. Our results are the first demonstration of a novel and promising method to generate programmable femtosecond waveforms down to the UV range. This method is also directly applicable to amplified femtosecond systems, where high nonlinear conversion efficiency should be possible. It can also be extended to sum-frequency generation, where shorter output wavelengths should be possible.

Acknowledgment

The authors would like to thank Raytheon Company, Waltham, MA for providing the 512-element LCM device.

References

[1] A. M. Weiner, "Femtosecond pulse shaping using spatial light modulators," *Rev. Sci. Instrum.*, vol. 71, pp. 1929–1960, May 2000.

[2] M. Hacker *et al.*, "Micromirror SLM for femtosecond pulse shaping in the ultraviolet," *Appl. Phys. B Photophys. Laser Chem.*, vol. 76, no. 6, pp. 711–714, June 2003.

[3] Y. Q. Liu, S. G. Park, and A. M. Weiner, "Enhancement of narrow-band terahertz radiation from photoconducting antennas by optical pulse shaping," *Opt. Lett.*, vol. 21, no. 21, pp. 1762–1764, Nov. 1996.

[4] F. Eickemeyer, R. A. Kaindl, M. Woerner, T. Elsaesser, and A. M. Weiner, "Controlled shaping of ultrafast electric field transients in the mid-infrared spectral range," *Opt. Lett.*, vol. 25, no. 19, pp. 1472–1474, Oct. 2000.

[5] T. Witte, D. Zeidler, D. Proch, K. L. Kompa, and M. Motzkus, "Programmable amplitude- and phase-modulated femtosecond laser pulses in the mid-infrared," *Opt. Lett.*, vol. 27, no. 2, pp. 131–133, Jan. 2002.

[6] H. S. Tan and W. S. Warren, "Mid-infrared pulse shaping by optical parametric amplification and its application to optical free induction decay measurement," *Opt. Express*, vol. 11, no. 9, pp. 1021–1028, May 2003.

[7] N. Belabas, J. P. Likforman, L. Canioni, B. Bousquet, and M. Joffre, "Coherent broadband pulse shaping in the mid-infrared," *Opt. Lett.*, vol. 26, no. 10, pp. 743–745, May 2001.

[8] M. Hacker, R. Netz, M. Roth, G. Stobrawa, T. Feurer, and R. Sauerbrey, "Frequency doubling of phase-modulated, ultrashort laser pulses," *Appl. Phys. B Photophys. Laser Chem.*, vol. 73, no. 3, pp. 273–277, Sept. 2001.

[9] Z. Zheng and A. M. Weiner, "Coherent control of second harmonic generation using spectrally phase coded femtosecond waveforms," *Chem. Phys. Lett.*, vol. 267, pp. 161–171, June 2001.

[10] C. V. Bennett and B. H. Kolner, "Principle of parametric temporal imaging – Part I," *IEEE J. Quantum Elect.*, vol. 36, pp. 430–437, Apr. 2000.

[11] ——, "Principle of parametric temporal imaging–Part II," *IEEE J. Quantum Elect.*, vol. 36, pp. 649–655, June 2000.

[12] A. Assion *et al.*, "Control of chemical reactions by feedback-optimized phase-shaped femtosecond laser pulses," *Science*, vol. 282, pp. 919–922, Oct. 1998.

[13] R. Bartels *et al.*, "Shaped pulse optimization of coherent emission of high-harmonic soft X-rays," *Nature*, vol. 405, pp. 164–166, July 2000.

[14] N. Dudovich, D. Oron, and Y. Silberberg, "Single-pulse coherently controlled nonlinear raman spectroscopy and microscopy," *Nature*, vol. 418, pp. 512–514, Aug. 2002.

[15] T. Brixner, N. H. Damrauer, P. Niklaus, and G. Gerber, "Photoselective adaptive femtosecond quantum control in the liquid phase," *Nature*, vol. 414, pp. 57–60, Nov. 2001.

[16] R. J. Levis, G. M. Menkir, and H. Rabitz, "Selective bond dissociation and rearrangement with optimally tailored, strong-field laser pulses," *Science*, vol. 292, pp. 709–713, Apr. 2001.

[17] S. Malinovskaya and P. Berman, "Coherent control of vibrational excitations by ultrafast pulse shaping," in *Abstracts of Papers of the American Chemical Society 226: 263-Phys. Part 2*, Sept. 2003.

[18] D. Goswami, "Optical pulse shaping approaches to coherent control," *Phys. Rep.*, vol. 374, no. 6, pp. 385–481, Feb. 2003.

[19] I. H. Chowdhury, X. Xu, and A. M. Weiner, "Ultrafast pulse train micromachining," in *Proc. SPIE*, vol. 4978, June 2003, p. 138.

[20] R. Stoian *et al.*, "Laser ablation of dielectrics with temporally shaped femtosecond pulses," *Appl. Phys. Lett.*, vol. 80, no. 3, pp. 353–355, Jan. 2002.

[21] J. Meijer *et al.*, "Laser machining by short and ultrashort pulses, state of the art and new opportunities in the age of the photons," *CIRP Annu. Manuf. Tech.*, vol. 51, no. 2, pp. 531–550, 2002.

[22] S. Nolte *et al.*, "Microstructuring with femtosecond lasers," *Adv. Eng. Mater.*, vol. 2, no. 1–2, pp. 23–27, Feb. 2000.

[23] J. Diels and W. Rudolph, *Ultrashort Laser Pulse Phenomena: Fundamentals, Techniques, and Applications on a Femtosecond Time Scale*. New York: Academic, 1996.

[24] K. Kato, "Tunable UV generation to 0.2325 μm in LiB_3O_5," *IEEE J. Quantum Elect.*, vol. 26, pp. 1173–1175, July 1990.

[25] G. Imeshev, A. Galvanauskas, D. Harter, M. A. Arbore, M. Proctor, and M. M. Fejer, "Engineerable femtosecond pulse shaping by second-harmonic generation with Fourier synthetic quasiphase-matching gratings," *Opt. Lett.*, vol. 23, no. 11, pp. 864–866, June 1998.

[26] H. Wang *et al.*, "20-fs pulse shaping with a 512-element phase only liquid crystal modulator," *IEEE J. Select. Topics Quantum Elect.*, vol. 7, pp. 718–727, July-Aug. 2001.

[27] D. A. Roberts, "Simplified characterization of uniaxial and biaxial nonlinear optical crystals—A plea for standardization of nomenclature and cenventions," *IEEE J Quantum Elect.*, vol. 28, pp. 2057–2074, Oct. 1992.

Haifeng Wang was born in Wuhan, China, in 1975. He received the B.S. degree in 1998 in electronic engineering from Tsinghua University, Beijing, China. In 2003, he received the Ph.D. degree in electrical and computer engineering from Purdue University, West Lafayette, IN.

His work on optical pulse shapers was presented at the Conference on Lasers and Electro-Optics (CLEO), Baltimore, MD, in 2001, and published in the IEEE JOURNAL OF SELECTED TOPICS IN QUANTUM ELECTRONICS. His work in type I second harmonic generation was presented at CLEO in 2003 and published in the IEEE JOURNAL OF Quantum ELECTRONICS. His main research interests include optical pulse shaping and nonlinear optics.

Andrew M. Weiner (S'84–M'84–SM'91–F'95) received the Sc.D. degree in electrical engineering from the Massachussets Institute of Technology (M.I.T.) in 1984.

From 1979 to 1984, he was a Fannie and John Hertz Foundation Graduate Fellow at M.I.T. In 1984, he joined Bellcore, one of the premier research organizations in the telecommunications industry at that time. In 1989, he was promoted to Manager of Ultrafast Optics and Optical Signal Processing. In 1992, he joined Purdue University, West Lafayette, IN, as Professor of Electrical and Computer Engineering. He is currently the Scifres Distinguished Professor of Electrical and Computer Engineering as well as ECE Director of Graduate Admissions. His research focuses on ultrafast optical signal processing and high-speed optical communications. He is especially well known for pioneering the field of femtosecond pulse shaping, which enables generation of nearly arbitrary ultrafast optical waveforms according to user specification.

Prof. Weiner has published four book chapters and over 120 journal articles. He has been author or coauthor of over 200 conference papers, including approximately 60 conference-invited talks, and has presented over 50 additional invited seminars at universities or industries. He holds five U.S. patents. He has received numerous awards for his research, including the Hertz Foundation Doctoral Thesis Prize (1984), the Adolph Lomb Medal of the Optical Society of America (1990), awarded for pioneering contributions to the field of optics made before the age of 30, the Curtis McGraw Research Award of the American Society of Engineering Education (1997), the International Commission on Optics Prize (1997), the IEEE LEOS William Streifer Scientific Achievement Award (1999), the Alexander von Humboldt Foundation Research Award for Senior U.S. Scientists (2000), and the inaugural Research Excellence Award from the School of Engineering at Purdue (2003). He is a Fellow of the Optical Society of America. He has served on or chaired numerous research review panels, professional society award committees, and conference program committees. In 1988–1989, he served as an IEEE Lasers and Electrooptics Society (LEOS) Distinguished Lecturer. He was General Co-Chair of the 1998 Conference on Lasers and Electrooptics, Chair of the 1999 Gordon Conference on Nonlinear Optics and Lasers, and Program Co-Chair of the 2002 International Conference on Ultrafast Phenomena. In addition, he has served as Associate Editor for IEEE JOURNAL OF QUANTUM ELECTRONICS, IEEE PHOTONICS TECHNOLOGY LETTERS, and *Optics Letters*. He served as an elected member of the Board of Governors of IEEE LEOS from 1997 to 1999 and as Secretary/Treasurer of IEEE LEOS from 2000 to 2002. He is currently a Vice-President (representing IEEE LEOS) of the International Commission on Optics (ICO).